

# **Imaging Autoclave Development for In-Situ Optical Measurement of High Temperature Aqueous Corrosion Processes**

P. M. Wood, J. A. Duff, T. J. Marrow

*Materials Performance Centre, School of Materials, The University of Manchester, Manchester, UK*

## Abstract

Stress corrosion cracking, oxidation and high temperature aqueous corrosion are life limiting factors in many nuclear process plant components. An Imaging Autoclave has been developed to study these processes, in-situ. The system combines refreshed-loop high temperature and pressure aqueous testing facilities under dynamic loading, with the optical techniques of Digital Image Correlation and Raman Spectroscopy. This paper reports an in-situ study of stress corrosion crack nucleation and growth in Stainless Steel under simulated BWR environments, using digital image correlation. This allows crack opening displacements to be measured that are below normal optical resolution. The aim is to measure crack propagation rates and determine nucleation sites.

## 1 INTRODUCTION

Stress Corrosion Cracking (SCC) and high temperature aqueous corrosion are significant degradation processes in many components in the nuclear power industry and in process plant. In these environments failure of structural mechanisms presents a substantial hazard to both safety and economic performance. Uncertainties in the kinetics of these damage mechanisms and their sensitivity to microstructure have a strong influence on lifetime prediction and arise due to both the complexity of the oxidation mechanisms and the difficulties of making in-situ experimental observations [1]-[4].

Some materials (e.g. stainless steels) used in these systems are generally resistant to corrosion by virtue of a thin self-healing film of oxide, but may be prone to cracking and localised corrosion under certain conditions [5], [6]. Other materials (e.g. zirconium alloys) undergo quite complex general corrosion mechanisms, with the development of thick oxide layers [7]. Our ability to study both the protective films and the development of thick oxide layers in conventional studies is limited by the need to remove the sample from the high-pressure, high-temperature aqueous environment in order to perform the examination under ambient conditions [5], [8], [9]. For environmentally assisted cracking, it can be very important for the sample to remain in the active environment throughout the observation of the cracking process, as the kinetics of crack development are sensitive to the development of the crack tip chemistry, which may differ from the bulk environment [10]. Interruption of testing for examination may interfere with this, and provide inaccurate measurements of crack development rates. It is highly desirable to be able to “see” into the sealed chamber, which is usually used for high temperature and pressure autoclave testing.

An Imaging Autoclave has therefore been developed to enable the in-situ optical observation of high temperature aqueous corrosion processes. This new research facility aims to apply the techniques of Digital Image Correlation (DIC) strain mapping and Raman spectroscopy under realistic environments, with 1:0 (uniaxial) stress and 1:1 (equi-axial) slow strain rate, static and cyclic loading, at sufficient temperature and pressure to allow characterisation of material degradation processes. In particular, we aim to observe stress corrosion cracking of stainless steel (including initiation, growth orientation and coalescence behaviour) and oxidation of zirconium based alloys.

In-situ Raman spectroscopy of oxide surfaces in an autoclave has been used previously to examine zirconium alloys and stainless steels [11]-[13]. Sapphire crystal windows in the Autoclave wall (thickness 4.5 mm) were used, with a 0.25 mm thick CVD (chemical vapour deposition) diamond disk to protect the sapphire from chemical degradation [13]. In-situ Raman spectroscopy has also been used to measure oxide rupture and strains in stainless steel during slow strain rate tests [14]. Image correlation has never been applied in an autoclave, but has been used in ambient environments to observe grain boundary plastic strains in polycrystalline metals [15], and to study the nucleation and growth of cracks [16]. An Autoclave system, suitable for optical imaging, has been demonstrated [17], achieving a resolution of 30  $\mu\text{m}$  through a 160 mm length cubic zirconia crystal window. Our aim in this new system was to significantly improve the optical resolution to allow digital image correlation of stress corrosion cracking, in-situ. This has been achieved. The system is also suitable for in-situ Raman spectroscopy, which will be reported in a future paper.

## 2 EXPERIMENTAL

### 2.1 Autoclave System

The Imaging Autoclave was designed and built by Cormet Testing Systems (Helsinki, Finland) to a specification by The University of Manchester. It is a modified 10 kN slow strain rate testing autoclave with a sapphire viewing window in the base; conditioned water is supplied from a recirculating loop by means of a high pressure pump. Figure 1 shows a cross-section of the autoclave and the specimen loading jig. The autoclave body is manufactured from AISI 316L stainless steel, with a volume of 0.9 litres. The design operating pressure is 40 bar, with a design operating temperature of 250°C.

The loading jig forms part of the autoclave base, and is designed to test 1:0 uniaxial bend specimens or bi-axial (cruciform) bend specimens. The load is applied via the push rod (2), which is sealed by the push rod slide bearing (1) to allow free movement of the rod without steam leakage. The load is controlled via an Interface 1210AF-2K-B load cell with a maximum rating of 10 kN. The main autoclave seal, (3) in Figure 1, is manufactured from 2 mm thick Goretex, with an outside diameter (OD) of 110 mm. A polished sapphire window is incorporated in the autoclave base. It has a 40 mm diameter and 8 mm thickness (4).

The recirculating loop conditions the water entering the autoclave. It is manufactured from AISI 316L Stainless Steel. The low pressure side has a maximum operating pressure and temperature of 3 bar and 40°C respectively, while the high pressure side has a design operating pressure and temperature of 40 bar and 250°C. Water is pumped from a 135 litre storage tank at a flow rate of up to 5 l/hr by means of a Prominent HP2 high-pressure pump. A circulation pump (Johnson MDR45P2) circulates water from the storage tank through water-chemistry analysers to allow monitoring and control. The analysers include a dissolved oxygen sensor, a dissolved hydrogen sensor (both Orbisphere 510 with a range of 0 to 1000 ppb) and a conductivity sensor (ABB, AC221 with a range 0 to 10 $\mu$ S/cm). The system can run under deoxygenated conditions, oxygenated conditions (1000 ppb max) or under hydrogenated conditions, controlled using the partial pressure of hydrogen within the storage tank.

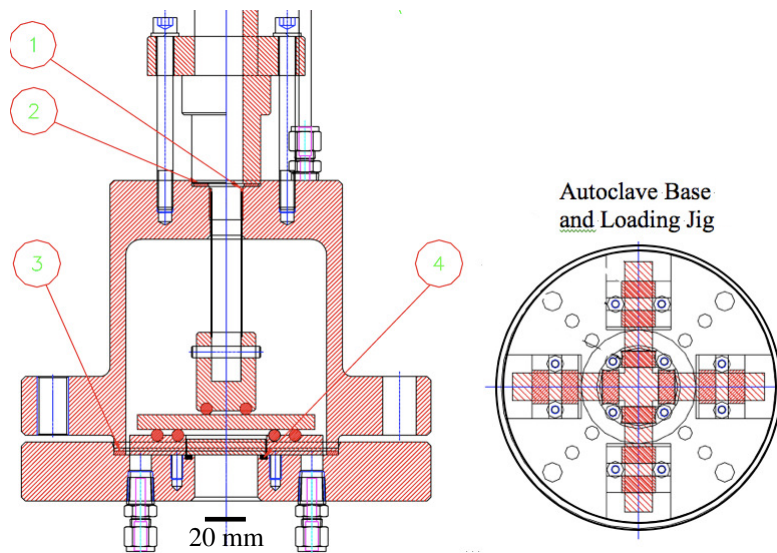


Figure 1: Autoclave and Base/Loading Jig. The position of the rollers for the outer loading spans can be changed, allowing 1:2 or 1:1 bi-axial loading with cruciform specimens, or to increase the moment available for higher strength specimens. Uni-axial four point bending can also be done. The sapphire window is indicated by label 4.

For oxygenated or deoxygenated autoclave input water, the flow from the circulation pump is configured such that water is taken from the storage tank and analysed directly. Automatic adjustment to control the oxygen content of the water in the storage tank is made by computer controlled magnetic valves from N<sub>2</sub> or N<sub>2</sub>/2%O<sub>2</sub> gas supplies. The flow loop can be reconfigured to allow analysis of the return water. Water purification is carried out by two ion exchange columns (Veolia Water Solutions and Technologies), which remove dissolved species directly from the storage tank water and also water returning from the autoclave. Chemical doping of the storage tank water may be achieved by an incorporated chemical mixing tank and circulation pump.

## 2.2 Optical Techniques

Digital Image Correlation is a technique for in-plane mapping of surface displacements by tracking of surface features in successive images. It is well suited to the observation and characterisation of surface breaking defects [16], but this technique has not previously been used to investigate stress corrosion cracking under high temperature aqueous conditions. It operates on optical images of the sample surface, obtained via a digital camera in the optical system. Digital image correlation was performed with an Image Pro X CCD camera (12 bit, up to 14 frames/second, 2048×2048 pixels) and a networked Dual Processor PC (2×2.8 Ghz Processors, 2 Gb RAM), with Davis Strain Master 2D software for acquisition and visualisation, (LA Vision, Germany). With a x20 objective lens, the field of view is approximately 450  $\mu\text{m}$  x 450  $\mu\text{m}$ , with an image pixel size of 0.23  $\mu\text{m}$ .

Raman Spectroscopy is non-contact and non-destructive and relies on the inelastic scattering of laser light from materials to give information about the specific chemical bonding. The technique can be used to measure elastic strains in oxide films under load [18] and study the development of oxide films [19]. The optical system was designed by Renishaw Ltd (Gloucester, UK), to the specification of The University of Manchester. It utilises an InVia Raman spectroscope with a Raman probe, allowing the transmission of the laser source to the specimen by means of a fibre-optic cable. It also incorporates a video camera for focusing of the Raman probe, and the higher specification camera for Digital Image Correlation. The excitation laser wavelength is 514 nm. The system also has a Leica microscope for standard Raman spectroscopy in which the illuminated spot size is 1-2  $\mu\text{m}$ .

Figure 2 shows the optical system with the Raman probe positioned beneath the autoclave window; (A) is the probe's microscope objective lens (x20, 13 mm working distance, manufactured by Zeiss), (B) is the Raman probe, with the microscope light source to the left, (C) is a high specification digital camera, (D) is the X-Y motorised stage (ProScan11, manufactured by Prior), and (E) is the fibre optic cable connection. Position control of the optical system by the X-Y stage allows surface mapping, within a range of  $\pm 4$  mm from the centre of the sapphire window. A mirror is used to switch the optical path between the Raman probe/laser, or the microscope light source/high specification camera for optical observation of the specimen surface.

## 2.3 Material

The Type 304 austenitic stainless steel (Cr:18.15, Ni:8.60, C:0.055, Mn:1.38, P:0.032, S:0.005, Si:0.45, N:0.038, Fe:Bal wt-%) was obtained as 13 mm plate and machined as rectangular uniaxial bend specimens (90 × 10 × 7.5 mm). The machined specimens were solution annealed at 1050°C for 2 hours in an air furnace and then air-cooled on a clean metal surface. It was then sensitised at 650°C for 24 hours, with heating and cooling as before. The specimen was

ground and polished to ¼ micron and electropolished with a 92% Acetic, 8% Perchloric Acid solution at 42V and 0°C. It was then electroetched with the Acetic/Perchloric Acid solution at 20V to provide sufficient features for digital image correlation. Finally, the specimen was immersed in a solution of 0.1M  $K_2S_4O_6$  at pH 2.5 for 14 hours, causing intergranular corrosion from which stress corrosion cracking could propagate.

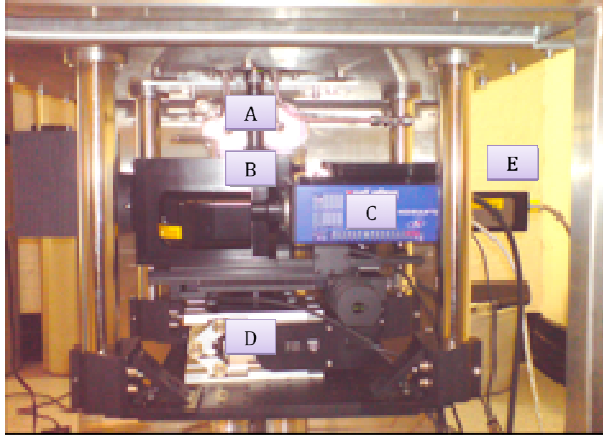


Figure 2: The optical system, positioned beneath the autoclave window, with (A) Microscope objective lens, (B) Raman probe body, (C) CCD camera for image correlation, (D) X-Y motorised stage and (E) Fibre optic cable connection.

### 3 IN-SITU OBSERVATION OF IGSCC BY IMAGE CORRELATION

Image correlation has previously been used to study intergranular stress corrosion crack nucleation and growth under ambient conditions [16]. The ultimate aim of this research is to study the role of environment, loading and microstructure in the development of the crack nucleus, leading to improved models for stress corrosion crack behaviour. The Image Correlation algorithm used in this study is implemented in commercial software developed by LaVision. It is based on Equation (1) [20]. Captured images are discretised into smaller interrogation windows across the time series. Individual interrogation windows at position  $(x,y)$  are converted via Fast Fourier Transform,  $I_1$ , and then compared with the transform of the interrogation window,  $I_2$ , in the subsequent image for a range of potential displacements  $(dx, dy)$ . The degree of correlation across various displacements is calculated,  $C(dx,dy)$  and the maximum correlation is used to identify the interrogation window displacement. Displacements for each interrogation window across the whole image can then be mapped and strains calculated by differentiation. Surface crack openings, which are smaller than the interrogation window size, are represented by a large localised effective strain.

$$C(dx, dy) = \sum I_1(x, y)I_2(x + dx, y + dy) \quad (1)$$

The autoclave was heated up to 250°C with oxygenated water at 1000 ppb flowing through the system. This approach was adopted, as it takes considerably

longer to oxygenate the water than to heat up the autoclave. Following heating of the autoclave to 250°C, the specimen was loaded to yield (200MPa) and then held at that static load for the duration of the test.

The autoclave window and water reduce the quality of the image. Figure 3A shows a sample viewed through the window with water at 250°C, compared to a similar sample viewed through the same optics but with the window removed (Figure 3B). To improve image quality, post processing of the images is carried out. Each observation consists of six images collected over 3 seconds. A sliding background subtraction [21] is performed to remove the effect of large variations in intensity across the whole image and then particle intensity normalisation [22] is carried out to highlight individual features on the sample surface. The six images are then averaged together to remove any transient variations that may have occurred during collection. Figure 3C shows Figure 3A after processing. The microstructure is clearly visible.

The image processing reduces the uncertainty in the displacement vectors to around 0.2 to 0.3 pixels (RMS noise obtained by correlation of successive observations of the same location. This is unaffected by moving the observation away from, and then back to this location using the X-Y stage). In the absence of the window and water, the RMS displacement noise was between 0.15 and 0.2 pixels for the same optics and sample preparation. (1 pixel is 0.23  $\mu\text{m}$ ).

No cracking was detected during the first 18 days of the test. However, the vertical displacement field (in pixels) obtained by correlation between the first image of the sample at the start of the test and at Day 19 is shown in Figure 4A. The applied stress direction in the figure is vertical. A displacement step of approximately 5 pixels is seen towards the bottom of the image. A minimum interrogation window size of 32x32 pixels with 25% overlap was used, thus the displacement vectors are obtained at intervals of approximately 5.5  $\mu\text{m}$ . This displacement step is judged to be due to a crack, which entered the field of view between the observations between day 18 and day 19.

Development of cracking is shown in Figure 4B to D. The orthogonal in-plane displacements have been differentiated to obtain the maximum normal strain, and the resulting strain map overlaid on an image of the microstructure. While the lower crack developed outside the field of view and remains stable, a smaller feature develops towards the middle of the image. The displacement measured across this feature when it first became visible was 0.1  $\mu\text{m}$ , increasing to 0.25  $\mu\text{m}$  at day 28.

Conventional optical microscopy of the unloaded sample in air after the test confirmed that image correlation had successfully detected the lower crack. A micrograph of the crack is shown in Figure 5, compared with the strain map obtained by image correlation. The second crack was not visible in the optical image, due to its small opening displacement and the removal of load at test end. Assuming the surface displacements are equivalent to crack opening

displacement, a maximum crack opening of  $0.1\ \mu\text{m}$  would result from a surface breaking semi-circular flaw with a depth of  $20\ \mu\text{m}$  at a tensile stress of  $200\ \text{MPa}$  ( $E=200\ \text{GPa}$ ,  $\nu=0.3$ ) [23]. This is comparable to the grain size. A crack opening of  $0.25\ \mu\text{m}$  is predicted for a crack depth of  $50\ \mu\text{m}$ . The predicted relationship between crack opening and crack depth is insensitive to the surface length. This observation demonstrates that the imaging system is suited for in-situ observation of stress corrosion cracks nuclei. The displacement noise is around  $0.05$  to  $0.07\ \mu\text{m}$ , so some smaller defects may be resolved. Work is in progress to confirm the actual crack depths.

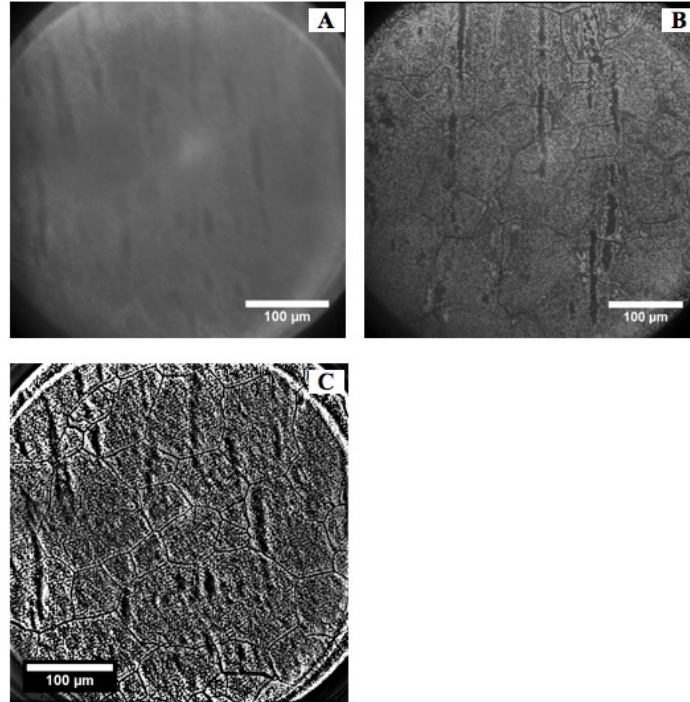


Figure 3: Observations of stainless steel: (A) Samples through sapphire window and water at  $250^{\circ}\text{C}$  (un-processed image), (B) Sample with no water or window, (C) Sample through sapphire window and water at  $250^{\circ}\text{C}$  (processed image).

In this experiment, a significant crack nucleated outside the chosen field of view. The precision X-Y stage allows control of camera position, and repositioning of the camera has no measurable effect on the errors in the displacement vector calculations. Scanning the camera to make observations over a larger area is a suitable method for crack growth observations, which will be employed in future tests.

#### 4 CONCLUSIONS

These preliminary results demonstrate that intergranular stress corrosion cracking in austenitic stainless steel can be observed and quantified by digital image correlation techniques. The optical system described in this paper is also suitable for in-situ observation of oxide development by Raman spectroscopy. Future

work will use this system to examine the kinetics of stress corrosion and corrosion fatigue crack initiation, growth and interaction.

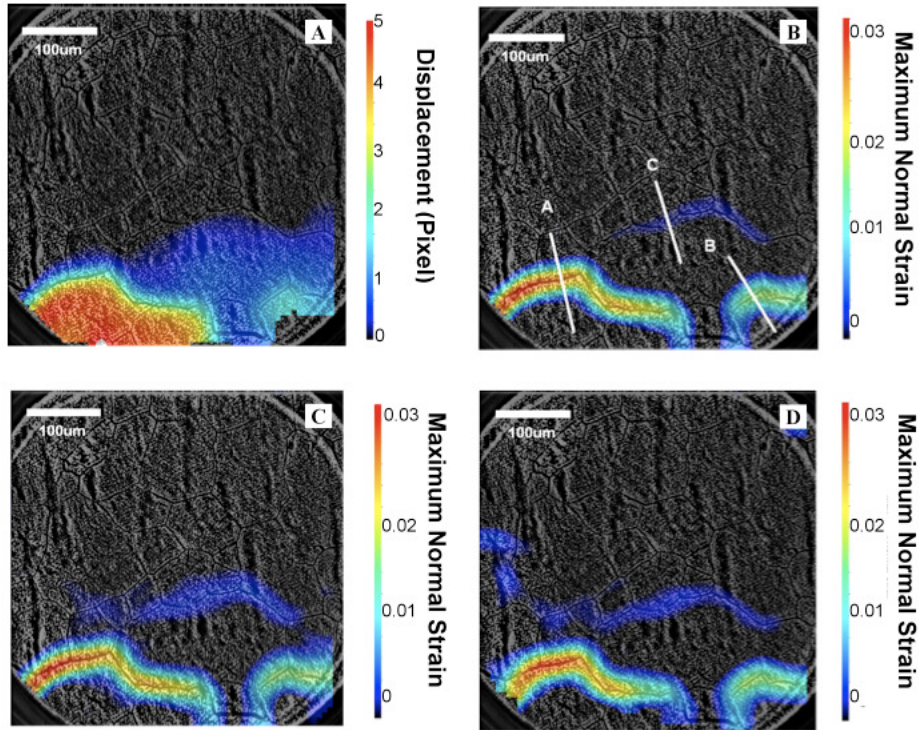


Figure 4: In-situ observations of crack nucleation in high temperature water. (A) displacements in pixels (1 pixel = 0.23  $\mu\text{m}$ ) in the vertical axis of the image, between images recorded at the start of the test and on Day 19. Strain maps obtained by correlation between the first image and those at (B) 19 days, (C) 23 days and (D) 28 days exposure in the autoclave.

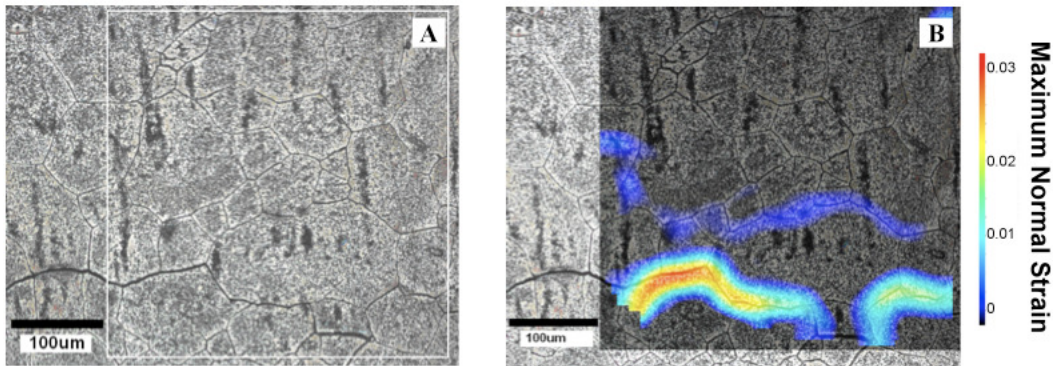


Figure 5: Optical microscopy (post-test). (A) The lower crack detected in Figure 4D is shown. The white box shows the area examined in-situ. (B) Overlay of strain map (at Day 28) on the ex-situ, post-test optical micrograph.

**Acknowledgments:** The authors are grateful to Rolls-Royce Ltd for their financial support of this project, and to both the Cormet Systems and Renishaw Ltd for their technical support.

## 5 REFERENCES

- [1] A. King, G. Johnson, D. Engelberg, W. Ludwig, J. Marrow, Observations of intergranular stress corrosion cracking in a grain-mapped polycrystal, *Science*, 321, (2008), 382-384
- [2] M. Kamaya, T. Haruna, Influence of local stress on initiation behaviour of stress corrosion cracking for sensitized 304 stainless steel, *Corrosion Science*, 49, (2007), 3303-3324
- [3] X. Liu, G.S. Frankel, B. Zoofan, S.I. Rokhlin, In-situ observation of intergranular stress corrosion cracking in AA2024-T3 under constant load conditions, *Corrosion Science*, 49, (2007), 139-148
- [4] J. Nakano, Y. Miwa, T. Tsukada, S. Endo, K. Hide, In situ SCC observation on neutron irradiated thermally-sensitized austenitic stainless steel, *Journal of Nuclear Materials*, 367-370, (2007), 940-946
- [5] B. Stellwag, The mechanism of oxide film formation on austenitic stainless steels in high temperature water, *Corrosion Science*, 40, (1998), 337-370
- [6] J. Robertson, The mechanism of high temperature aqueous corrosion of stainless steels, *Corrosion Science*, 32 (4), (1991), 443-465
- [7] C. Lemaignan, Corrosion of zirconium alloy components in light water reactors, in: S.D. Cramer, B.S. Corvino, *ASM Handbook Volume 13C Corrosion: Environments and Industries*, ASM International, (2006), 415-420
- [8] P. Barberis, T. Merle-Mejean, P. Quintard, On Raman spectroscopy of zirconium oxide films, *Journal of Nuclear Materials*, 246, (1997), 232-243
- [9] Z. Lu, T. Shoji, Y. Takeda, Y. Ito, A. Kai, S. Yamazaki, Transient and steady state crack growth kinetics for stress corrosion cracking of a cold worked 316L stainless steel in oxygenated pure water at different temperatures, *Corrosion Science*, 50, (2008), 561-575
- [10] A. Turnbull, Modelling of environment assisted cracking, *Corrosion Science*, 34, (1993), 921-928
- [11] J.E. Maslar, W.S. Hurst, W.J. Bowers, J.H. Hendricks, In situ Raman spectroscopic investigation of zirconium-niobium alloy corrosion under hydrothermal conditions, *Journal of Nuclear Materials*, 298 (3), (2001), 239-247
- [12] J. Mougou, A. Galerie, M. Dupeux, N. Rosman, G. Lucazeau, A.M. Huntz, L. Antoni, In-situ determination of growth and thermal stresses in chromia scales formed on a ferritic stainless steel, *Materials and Corrosion*, 53, (2002), 486-490
- [13] J.H. Kim and I.S. Hwang, In-situ Raman spectroscopic study of oxide films on Alloy 600 in simulated PWR water, *Proceedings of the 11th Int. Conf. Environmental Degradation of Materials in Nuclear Systems*, Stevenson, USA, (2003)
- [14] A. Kai, M. Takegoshi, T. Shoji, In situ Micro Raman Spectroscopy for characterization of oxide film formed on the new surface and for measurements of the stress of oxide film formed on 304L stainless steel, *Key Engineering Materials*, 261-263, (2004), 913-918
- [15] J. Quinta da Fonseca, P.M. Mummery and P.J. Withers, Full-field strain

mapping by optical correlation of micrographs acquired during deformation, *Journal of Microscopy*, 218, (2005), 9–21

[16] J.A. Duff, T.J. Marrow, In-situ observations of intergranular stress corrosion cracking, *Proceedings of the 2008 ASME Pressure Vessels and Piping Conference*, Chicago, USA, (2008). Paper PVP2008-61208.

[17] T. Fukumora, N. Nakajima, N. Totsuka, M. Okada, Development of an Autoclave with zirconia windows for in-situ observation of sample surface under the primary water conditions of pressurized water reactors, *Journal of Nuclear Science Technology*, 39 (3), (2002), 276-278

[18] G. Hilson, K.R. Hallam, P.E.J. Flewitt, The measurement of stresses within oxides produced on austenitic and ferritic steels using Raman spectroscopy, *Materials Science Forums*, 524-525, (2006), 957-962

[19] P. Bouvier, J. Godlewski, G. Lucazeau, A Raman study of the nanocrystallite size effect on the pressure-temperature phase diagram of zirconia grown by zirconium-based alloys oxidation, *Journal of Nuclear Materials*, 300, (2002), 118-126

[20] O. Ronneberger, M. Raffel, J. Kompenhans, Advanced Evaluation Algorithms for standard and dual plane particle image velocimetry, *Proc 9th International Symposium on applications of Laser techniques to Fluid Mechanics*, (1998) Lisbon July, 10.1

[21] R.C. Gonzalez and R.E. Woods, *Digital Image Processing: Second Edition*, Prentice Hall, New Jersey, (2002), 103

[22] Q.Z. Wu, B.S. Jeng, Background subtraction based on logarithmic intensities, *Pattern Recognition Letters*, 23(13), (2002), 1529-1536

[23] J.E. Hack, and G.R. Leverant, On the prediction of the surface crack opening displacement of a part through crack, *International Journal of Fracture*, (1980) 16(1), 15-18